$\mu = 14.0\times10^{-18}$ esu cm, and $T = 40\,^{\circ}$K, we obtain

$$\tan\delta \simeq 0.8/\omega\tau .$$

This value is consistent with our data, from which we can estimate a $\tan\delta$ maximum of about 10^{-3}. Thus we see that the temperature-dependent part of the dielectric-mode relaxation rate $1/t_d$ is related to the electron-hopping rate $1/\tau$, and gives us

$$\tau = (0.67\times10^{-10})e^{220/T} .$$

The dipole moment that was used above is based on the c-axis hopping-electron model of Dominik and MacCrone.[3] The hopping electron associated with the vanadium impurity is similar to process III of Dominik and MacCrone.

In this model the electron is first associated with the V^{+5} core to form a paramagnetic V^{+4} ion. With the help of thermal excitation, the electron can jump to the nearest Ti^{+4} core, which is along the c axis and 2.96 Å away. This then forms the Ti^{+3} ion, which is also paramagnetic. The hopping of the electron between the V^{+4} state and the Ti^{+3} state is the process that we believe is responsible for our dielectric loss.

Our spin-echo work also shows this because the spin-echo amplitude decreases as the dielectric loss increases. Since the g values of the Ti^{+3} and V^{+4} ions are different and the hopping is not fast enough to cause motional narrowing, we observe the spin-echo signal only from the vanadium sites. The transverse relaxation time is 7.0 μsec.

The crystal was annealed in air to remove oxygen vacancies but this had little effect on the dielectric loss. This indicates that no oxygen vacancy is associated with the vanadium impurities.

ACKNOWLEDGMENT

The author wishes to thank Bill Rumpp for making the dielectric-loss measurements.

*Work supported by the Materials Research Center, University of North Carolina under Contract No. DAHC15-67-C-0223 with the Advanced Research Projects Agency.

[1]F. A. Grant, Rev. Mod. Phys. 31, 646 (1959).

[2]A. Von Hippel, J. Kalnajs, and W. B. Westphal, J. Phys. Chem. Solids 23, 779 (1962).

[3]L. A. K. Dominik and R. K. MacCrone, Phys. Rev. 156, 910 (1967); 163, 756 (1967).

[4]Edward S. Sabisky and Hendrik J. Gerritsen, J. Appl. Phys. 33, 1450 (1962).

[5]S. Ramo and J. R. Whinnery, *Fields and Waves Modern Radio* (Wiley, New York, 1953), pp. 388–393.

[6]E. L. Hahn, Phys. Rev. 80, 580 (1950).

[7]R. L. Sanders and L. G. Rowan, Phys. Rev. B 4, 2099 (1971).

[8]H. Frohlich, *Theory of Dielectric* (Oxford U.P., New York, 1958), pp. 73–75, 91–98, and 121–122.

PHYSICAL REVIEW B VOLUME 5, NUMBER 5 1 MARCH 1972

First- and Second-Shell Hyperfine Interactions in Iron-Group-Doped Perovskite Fluorides

R. K. Jeck* and J. J. Krebs
Naval Research Laboratory, Washington, D.C. 20390
(Received 23 September 1971)

An electron-spin-resonance (ESR)/electron-nuclear double-resonance (ENDOR) investigation of $KZnF_3:M$ ($M = Mn^{2+}$, Fe^{3+}, Co^{2+}, Ni^{2+}) has been carried out with a view toward obtaining an improved understanding of the second-neighbor fluorine (F2) hyperfine interaction in perovskite hosts. The isotropic part of the F2 hyperfine interaction is calculated using the "overlap" model of Davies and improved fluorine-ion wave functions. The results are compared with both the present experiment and recently published data for V^{2+}, Cr^{3+}, Mn^{2+}, and Cr^{1+} in $KMgF_3$. This comparison indicates that the overlap model by itself is inadequate and that covalency effects are of comparable importance for the F2 ions. In addition to the F2 results for Mn^{2+} and Fe^{3+}, we report ESR and precise ENDOR measurements of the nearest-neighbor fluorine, the ^{55}Mn, and the ^{59}Co hyperfine interactions. The modified nuclear g factor found for $^{59}Co^{2+}$ is shown to be consistent with theory.

I. INTRODUCTION

The electron-spin-resonance (ESR) spectra of $3d^n$ ions in fluoride host crystals are characterized by prominent superhyperfine (shf) structure which arises from the transferred hyperfine interaction[1] with the nearest-neighbor (nn) fluorine ligands. A number of papers have dealt with the problem of explaining the details of this type of interaction in a variety of complexes.[2,3] One reason for this interest is the realization that these shf interactions are related to the still imperfectly understood mecha-

nisms of superexchange in magnetically ordered compounds.[2,4-6]

The primary interest of the present paper is in the interaction of the $3d^n$ ions with fluorine ions more distant than nn. These distant ligands produce only a line broadening of the ESR spectra, but the use of electron-nuclear double resonance (ENDOR) allows these smaller interactions to be probed quantitatively. Davies[7] used ENDOR to examine the next-nearest-neighbor (nnn) fluorine shf interaction with V^{2+} and Mn^{2+} in the cubic perovskite $KMgF_3$ and treated the results in terms of the overlap between the orbitals of the nnn fluorines (F2) and the partially spin-polarized orbitals of the nn fluorines (F1). In order to further test this model, we have extended the ENDOR studies to include the isoelectronic ions Mn^{2+} and Fe^{3+} in $KZnF_3$. This cubic salt is expected to be somewhat more covalent than $KMgF_3$ due to the smaller electronegativity difference between Zn and F as compared to Mg and F. While this work was in progress, Davies and Horai[8] (hereafter referred to as DH) completed ENDOR studies on F2 neighbors of Cr^+ and Cr^{3+} in $KMgF_3$.

In examining the accumulated F2 data, we were led to repeat the calculations of Davies and DH and found that the F^- wave functions they used were inadequate. Using better wave functions, we have recomputed the F1-F2 overlap contributions to the F2 shf interaction for V^{2+}, Cr^{3+}, Cr^+, and Mn^{2+} in $KMgF_3$ and for Fe^{3+} and Mn^{2+} in $KZnF_3$ and have compared the results with experiment and previous calculations.[7,8] This comparison suggests that covalency plays a significant role in the observed F2 interaction. In addition to the F2 results, we report a number of ENDOR and ESR measurements of other spin-Hamiltonian parameters for Mn^{2+}, Fe^{3+}, Co^{2+}, and Ni^{2+} in $KZnF_3$. A preliminary account of the $KZnF_3:Mn^{2+}$ work has been published previously.[9]

We would like to emphasize that a good amount of data on F2 shf interaction in the perovskite fluorides has now accumulated. Although the correct order of magnitude is usually explained by the overlap model, the model is clearly deficient in neglecting covalency. It would seem that the time is ripe for a more thoroughgoing theoretical calculation which would try to estimate the F2 shf constant on an *ab initio* basis. The rather simple structure and high symmetry of these crystals offers further encouragement for such an endeavor.

II. EXPERIMENTAL APPARATUS AND PROCEDURE

A. Apparatus

The K_u-band ESR/ENDOR spectrometer used for these experiments operates in a homodyne mode and uses a cylindrical microwave cavity operating in the TE_{011} mode with a resonant frequency near 16.1 GHz. The degenerate TM_{111} mode was suppressed by using the method of Cook *et al.*[10] The simple adjustable cavity-to-waveguide coupling was patterned after the design of Gordon[11] in which a movable Teflon slug is positioned in a section of "below cutoff" waveguide just above the coupling iris. The coupler was adjusted by a stiff rod linked to the Teflon, with the upper end passing through an O-ring seal in the Dewar header. The use of a separate waveguide arm and a hybrid Tee to deliver bias power to the microwave detector allowed separate detector diodes to be used for the ESR and the automatic frequency control signals. This arrangement reduced the amount of rf pickup interference with the ENDOR measurements. A low-noise Schottky diode (MA 4861D) was used to detect the ESR/ENDOR signals.

The single-crystal samples were held in the center of the cavity by means of a small polystyrene platform, the bottom of which was threaded to screw onto the head of a Microdot coaxial connector. This connector itself threaded into a hole in the bottom plate of the cavity, an arrangement which allowed easy insertion of the samples as well as the ability to exchange samples while affecting only their rotational orientation about the vertical axis. The sample was mounted by securing it to the top of the platform with rubber cement and then winding a 3–5 turn coil of No. 36 wire around it. A shallow trench machined along a diameter of the platform top provided room for the turns of the coil to pass under the sample without affecting its seating. A hole drilled axially through the stem of the platform allowed one lead from the coil to pass through while the ground lead passed down the outside of the platform stem to the shank of the Microdot connector. Although this arrangement reduced the cavity Q somewhat, the reduction was tolerable.

The rf oscillator was a motor-driven Hewlett Packard model No. 608D signal generator. Amplification of the rf was provided by two broad-band amplifiers in series—a Hewlett Packard model No. 460AR, followed by an Instruments for Industry model No. 500A. This combination was capable of delivering an estimated 5 W of rf power to the sample coil at frequencies where the impedance match between the amplifers and the sample coil was maximum.

B. Procedure

The crystal samples were obtained from boules grown from the melt in our laboratory. The concentration of transition-metal ions relative to zinc ions was nominally 0.05% in most cases. Irregularly shaped single-crystal pieces "mined" from the boules were oriented either by standard x-ray techniques or by means of cleavage-face reflections using a low-power laser. The crystal was then cut

as a small block having {100} faces 3–4 mm on a side.

Final adjustments to align a [100] direction parallel to the applied magnetic field $\vec{H}$ were made by rotating the magnet and observing either the Mn^{2+} or Fe^{3+} ESR, one of which was always present at least as a trace impurity, or by observing the splitting of the F2 ENDOR signals. The latter provided a more sensitive indication of misalignment with a tilt of only 0.5° being readily apparent.

In order to observe the ENDOR signals, the field modulation was switched off and 100% amplitude-modulated (AM) rf was applied to the sample coil. The AM frequency was either 14 or 3.8 KHz, the latter usually giving a slightly better signal resolution but a slightly poorer signal-to-noise ratio. The ENDOR signal intensities were maximized by tuning the rf oscillator to a given ENDOR transition and then optimizing various experimental parameters, such as the applied field strength and the microwave power level. The optimum microwave power level was found to be near that value which gives a maximum in the plot of ESR signal intensity vs microwave power level.

The F1 hyperfine interaction constants $A_{\parallel}$ and $A_{\perp}$ (see the Appendix) were computed from ENDOR frequencies measured with $\vec{H} \parallel [100]$. By selecting in turn the proper ESR transitions, one could measure ENDOR signals corresponding to various values of $M = \langle S_Z \rangle$. The ENDOR signals were recorded vs frequency by placing frequency markers on the chart as the rf was scanned over a given range. The crystal calibrator internal to the HP 608D allowed for frequency markers to be accurately placed at 1-MHz intervals. Precise measurements of ENDOR frequencies were obtained by manually tuning the rf oscillator to the center of individual ENDOR transitions and measuring the frequency with a counter.

For the F2 nuclei, the hyperfine tensor $\overleftrightarrow{B}$ (see the Appendix) is not diagonal in the cube-edge coordinate system as it is for the F1 fluorines. In order to evaluate the two off-diagonal components B_{xz} and $B_{zx'}$, angular-dependent data were obtained and the hyperfine components B_{ij} were then evaluated from a computerized least-squares fit of the frequency equations to the data. Due to the large number of F2 ENDOR transitions at orientations other than $\vec{H} \parallel [100]$, it was impractical to measure them manually. Instead, frequency markers were used as mentioned above, and the ENDOR frequencies were obtained from the recorded spectrum by interpolation. This method was accurate to within 20 kHz.

III. EXPERIMENTAL RESULTS

For reference purposes, the spin Hamiltonian and the resonance equations appropriate to these perovskite complexes are presented in the Appendix. The unit cell and the labeling scheme used for the nn and nnn ligands are illustrated in Fig. 1. Results for the various ions are summarized in Tables I and II.

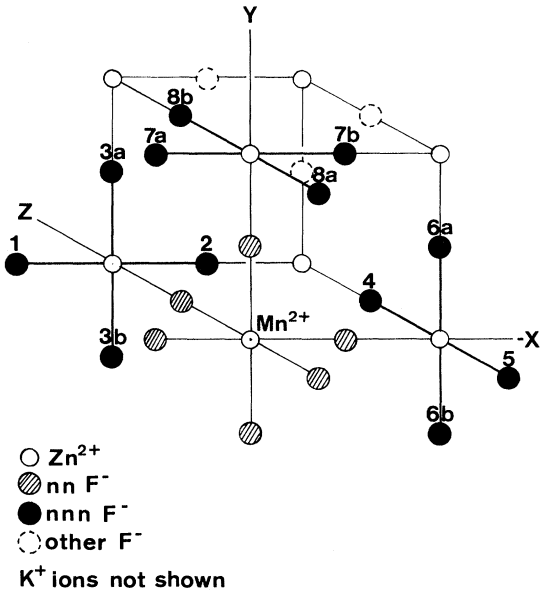

FIG. 1. Perovskite crystal structure and numbering scheme used for the nnn (F2) ligands.

A. $KZnF_3:Co^{2+}$ System

The Co^{2+} ESR spectrum was observable only at liquid-helium temperature (LHeT) and displayed well-resolved F1 shf structure. The ENDOR spectra from the type-II fluorines (defined as those four F1 fluorines in the plane perpendicular to $\vec{H}$ with $\vec{H} \parallel [100]$), are complicated by the presence of the multiplet structure shown in Fig. 2. Similar spectra have been observed by Kravitz and Piper[12] (hereafter referred to as KP) in the ^{19}F ENDOR spectrum of an $(FeF_6)^{3-}$ complex in CdTe. These authors explained the structure as arising from an indirect nuclear spin-spin interaction between the type-II fluorines. The theory of KP has been extended in the Appendix of the present article to include the effects of the central ion hyperfine interaction. Thus, the shf constants $A_{\parallel}$ and $A_{\perp}$ were evaluated by substituting the F1 ENDOR frequencies into Eqs. (A9) and (A11), respectively, and these results are presented in Table I. The theoretical ENDOR spectrum computed from Eq. (A12) is shown as a stick diagram in Fig. 2. The position of the multiplet components and their relative intensities (computed assuming the ENDOR transitions are not saturated) are in good agreement with experiment. It should be noted that these intensities differ from those indicated by KP. The ap-

TABLE I. Experimental spin-resonance parameters. All entries (except g, f_s, and $f_\sigma - f_\pi$) are in units of 10^{-4} cm^{-1}. The number in parentheses following an entry denotes the units of uncertainty in the last decimal places shown. Three dots indicates an unmeasured or nonexistent quantity. Unless otherwise noted, all LHeT hyperfine constants were determined by ENDOR. The LNT results differed negligibly from those at LHeT.

Temp	g	a	$^D A$	$A_\parallel$	$A_\perp$	f_s[a] (%)	$f_\sigma - f_\pi$[a] (%)
			$KZnF_3 : {}^{55}Mn^{2+}$				
RT	•••	6.3(1)[b]	−89.9(4)[d]	23.6(2)[b]	14.3(2)[b]	0.58	0.35
LHeT	2.0021(5)	6.9(1)[c]	−90.80(13)	24.19(2)	15.054(7)	0.60	0.26
			$KZnF_3 : Fe^{3+}$				
RT	2.0030(3)	52.7(2)[d]	•••	35.4(5)[d]	17.5(3)[d]	0.78	2.92
LHeT	•••	56.9(2)[d]	•••	35.99(2)	17.192(7)	0.78	3.20
			$KZnF_3 : {}^{59}Co^{2+}$				
LHeT	4.376(4)	•••	108.19(2)[e]	76.85(3)	27.07(4)	f	f
			$KZnF_3 : Ni^{2+}$				
LHeT	2.287(2)	•••	•••	64.7(5)[d]	25.8(10)[d]	0.56[g]	3.38[g]

[a]The fractional spin unpairing parameters were computed as in Ref. 2 using $R = 2.065$ Å for Mn^{2+}, $R = 1.92$ Å for Fe^{3+}, and $R = 2.01$ Å for Ni^{2+}, and are in line with values obtained from other pervokites listed in Appendix 3 of Ref. 2.

[b]Determined using computer-simulated first-derivative ESR spectra.

[c]Assumed unchanged from that measured at LNT.

[d]Evaluated directly from the ESR spectra.

[e]For Co^{2+} there is a modified ^{59}Co nuclear g factor g_n' with $g_n'/g_n = 1.44(1)$ (see text).

[f]See J. H. M. Thornley, C. G. Windsor, and J. Owen, Proc. Roy. Soc. (London) A284, 252 (1965) for a detailed account of how these are evaluated for the Co^{2+} ion.

[g]See Ref. 17 for orbital corrections used here.

pearance of the weak lines whose positions are marked by arrows shows that the small misorientation of this sample (1.2°) has increased the state admixtures sufficiently to make the $^1(A_{1g})_0 - {}^5(A_{1g})_{\pm 1}$ transitions[12] observable. The various multiplet components were found to have a full width at half-maximum (FWHM) of about 180 kHz.

No F 2 ENDOR could be detected in the Co^{2+}-doped samples.

In order to evaluate the Co hyperfine parameter ^{59}A from the ^{59}Co ENDOR data, it was necessary to take into account the modified nuclear g factor which arises because of the orbitally degenerate ground state of the Co^{2+} ion in octahedral coordination.[13] In the presence of the cubic field and spin-orbit interactions the lowest-lying substate of the Co^{2+} ion is a twofold degenerate Γ_6 state and there is a large orbital contribution to the hyperfine interaction. An applied magnetic field admixes upper levels of the ground $^4T_1$ manifold into the Γ_6 doublet in which ESR is observed. The resultant change in the magnetic moment produces a change, proportional to the applied field, in the hyperfine field at the cobalt nucleus. This effect may be expressed in terms of a modified nuclear g factor g_n' such that the spin Hamiltonian reads

$$\mathcal{H} = g\,\mu_B\,\vec{H}\cdot\vec{S} + {}^{59}A\,\vec{I}\cdot\vec{S} - g_n'\,\mu_N\,\vec{H}\cdot\vec{I} + \text{ligand terms}\ .$$

A least-squares analysis of the center frequencies of the broad (~1.2-MHz FWHM) ^{59}Co ENDOR transitions yields

$$^{59}A = (108.19 \pm 0.02)\times 10^{-4}\,\text{cm}^{-1},\quad g_n'/g_n = 1.44 \pm 0.01\ .$$

One can compute the ratio g_n'/g_n by combining the formulas of Pryce[13] to obtain

$$\frac{g_n'}{g_n} = 1 + \frac{40}{27}\,\frac{k\alpha + 2}{k\alpha}\left|\frac{^{59}A}{\lambda}\right|\frac{\mu_B}{\mu_N}\,g_n^{-1}R\ , \tag{1}$$

in which

$$R = \frac{\alpha - \kappa + \frac{13}{420}(1 - 15\tau^2)}{\frac{4}{3}\alpha - \frac{10}{3}\kappa + \frac{2}{63}(1 - 15\tau^2)} \tag{2}$$

and $-\alpha$ is the effective orbital angular momentum

TABLE II. Experimentally determined values of the shf tensor components for the F 2 nuclei at LHeT. All entries are in units of MHz. The numbers in parentheses following an entry denote the units of uncertainty in the last two decimal places shown. The components refer to the coordinate system in Fig. 1.

	$KZnF_3 : Fe^{3+}$	$KZnF_3 : Mn^{2+}$	$KMgF_3 : Mn^{2+}$[a]
B_{xx}	0.431 (12)	0.385 (31)	−0.067
B_{yy}	−0.497 (23)	−0.301 (40)	−0.651
B_{zz}	1.563 (08)	1.595 (15)	1.384
$\frac{1}{2}(B_{xz} + B_{zx})$	1.200 (08)	1.042 (16)	1.050
B_s	0.499 (14)	0.560 (18)	0.222

[a]From Ref. 7 with entries converted to the coordinate system of the present paper.

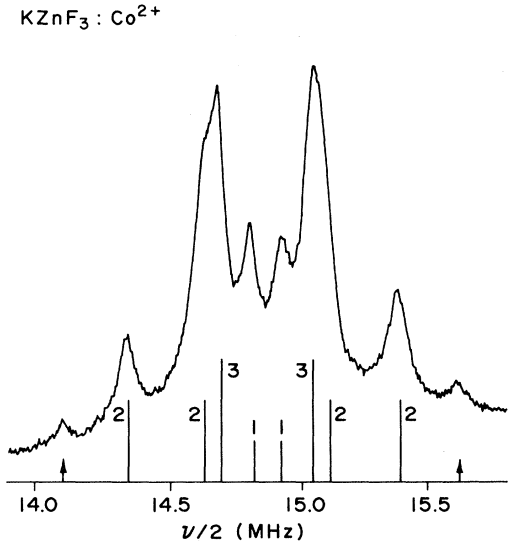

FIG. 2. Multiplet structure on the type-II F 1 ENDOR in $KZnF_3:Co^{2+}$. The line spectrum is computed using Eq. (A12) and the theoretical relative intensities are indicated.

associated with the triply degenerate orbital state of the cobalt ion in the crystal field, κ is the core-polarization constant (0.32),[13] λ is the spin-orbit coupling constant, k is the orbital-reduction factor, and τ gives the amount of ^4P level admixed into the ^4F ground state. The optical data[14] on $KMgF_3:Co^{2+}$ give $\alpha = 1.428$, $\tau = 0.17$, $\lambda = -167\ \mathrm{cm}^{-1}$, and $\Delta = 8000\ \mathrm{cm}^{-1}$, which along with the measured value of g in $KZnF_3:Co^{2+}$ (Table I) can be inserted into the equation[13]

$$g = \tfrac{10}{3} + (\tfrac{2}{3}\alpha - 15\lambda/2\Delta)k$$

to obtain $k = 0.940$. Equation (1) then gives $g_n'/g_n = 1.438$, in excellent agreement with experiment.

B. $KZnF_3:Mn^{2+}$ System

The Mn^{2+} ESR spectrum was recorded for $\vec{H} \parallel [100]$ at room temperature (RT), liquid-nitrogen temperature (LNT), and LHeT. Since the spectrum was complicated as usual by considerable overlapping of lines, the RT values of the cubic field parameter a and the shf constants $A_\parallel$ and $A_\perp$ were obtained by using a computer to simulate an ESR first-derivative spectrum which could be superimposed on the experimental spectrum and compared visually. The computer program made use of a resonance equation with terms carried to second order in the F 1 and ^{55}Mn hyperfine constants, the latter being evaluated independently from the experimental spectrum. At LNT, the ^{55}Mn and F 1 ENDOR transitions were observable with good signal-to-noise ratio so that the values of ^{55}A, $A_\parallel$, and $A_\perp$ determined from ENDOR frequencies were used in the computer program for generating the ESR spectrum. Thus, at LNT only the linewidth and the cubic field parameter a were varied to reproduce the spectrum. As at RT, Lorentzian line shapes gave a better reproduction of the observed ESR spectrum than did Gaussian shapes. The FWHM linewidths for both the ^{55}Mn and F 1 ENDOR ranged from ~400 kHz at LNT to ~150 kHz at LHeT, while the F 2 lines, observable only at LHeT, were about 50 kHz wide. The multiplet structure associated with type-II ENDOR lines was also present in the Mn^{2+}-doped samples at LHeT but was not well resolved.

The broad-band amplifiers used in our apparatus limited us to frequencies below 230 MHz so that only the ^{55}Mn ENDOR transitions corresponding to $M = \pm\frac{1}{2}$ could be observed. However, since the value of the nuclear-spin quantum number m affects the ENDOR frequency in second and third order, 12 different ^{55}Mn transitions can actually be observed corresponding to all allowable combinations of $M = \pm\frac{1}{2}$ and m. In all cases, except for $m = \pm\frac{5}{2}$, the ENDOR signal is found to be a doublet since the nuclear transitions giving rise to the signal can be either of the type $m \leftrightarrow m+1$ or $m \leftrightarrow m-1$.

The angular dependence of the F 2 ENDOR signals, examples of which are shown in Fig. 3, is derived in the Appendix. The components B_{ij} of the F 2 shf tensor were evaluated using a computerized least-squares fit of Eqs. (A16)–(A19) to angular-dependent data[9] similar to that shown in Fig. 4. The known sign of the Mn^{2+}-F 2 dipolar interaction allows one to determine the absolute sign of the results listed in Table II.

In principle, with six possible values of M in the Mn^{2+} case, there are also six possible sets of F 2 ENDOR transitions, each set being composed of

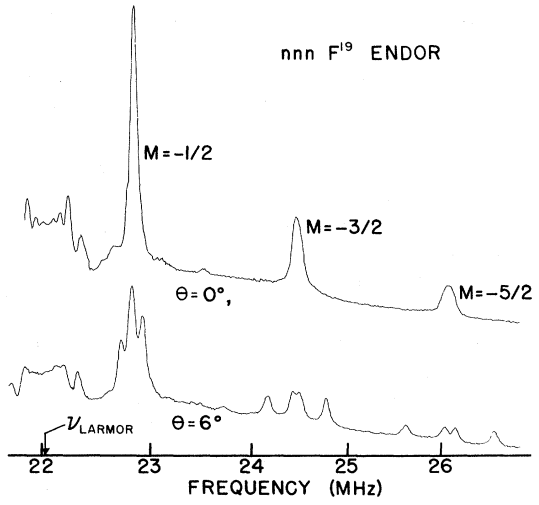

FIG. 3. Part of the F 2 ENDOR spectrum of $KZnF_3:Mn^{2+}$ at 4.2 °K. The angle θ is between H and [001] in the (010) plane.

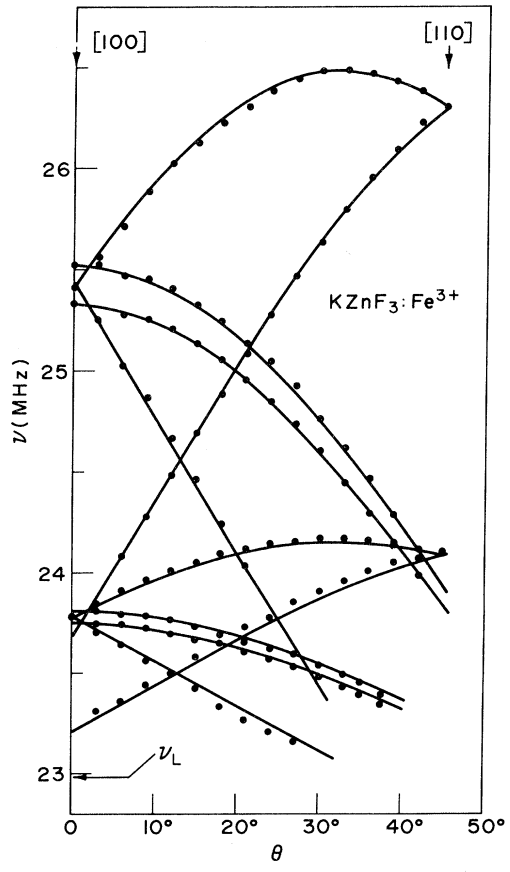

FIG. 4. Angular dependence of the F 2 ENDOR spectrum from $KZnF_3:Fe^{3+}$ at 4.2 °K. For clarity, only the lines corresponding to $\langle S_z\rangle = M = -\frac{1}{2}$ (lower set) and $M = -\frac{3}{2}$ (upper set) are shown. The doublet in each set results from a small (1.2°) sample misorientation. The solid lines are computed using the appropriate parameters in Table II. The angle θ is defined as in Fig. 3.

transitions of the type described by Eqs. (A16)–(A19). The three sets belonging to $M < 0$ occur at frequencies above the ^{19}F Larmor frequency ν_L and those corresponding to $M > 0$ occur below. The lower-frequency sets were found to be noticeably less intense than the ones above ν_L, a phenomenon which has been commented on by other authors.[15,16] If the ESR lines were pure and did not overlap or cross relax with one another, then when an ESR line associated with the transition $M \rightarrow M+1$ is pumped, only the two sets of ENDOR transitions corresponding to M and $M+1$ should appear. In practice, all six sets of F2 ENDOR signals could be seen simultaneously, irrespective of which Mn^{2+} ESR line was being used. However, the relative intensity of a given ENDOR set, such as the $M = -\frac{3}{2}$ group, for example, could be increased by pumping the proper ESR line. This procedure was sometimes helpful in identifying ENDOR lines which were overlapping or which were crowded together near the Larmor frequency.

Finally, we mention in passing that an unsuccessful attempt was made to detect ^{39}K ENDOR signals which were expected to occur no farther than a few MHz from the ^{39}K Larmor frequency near 1 MHz.

C. $KZnF_3:Fe^{3+}$ System

The Fe^{3+} ESR spectrum was recorded for $\vec{H} \parallel [100]$ at RT, LNT, and LHeT. In samples containing small amounts of iron, (~ 0.01% Fe^{3+}), the F1 shf structure was well resolved and the values of the resonance parameters a, $A_\parallel$, and $A_\perp$ were computed easily from the observed ESR spectrum. The F1 and F2 ENDOR signals were detected only at LHeT, where their linewidths were about 120 and 40 kHz, respectively. The LHeT values of the shf constants $A_\parallel$ and $A_\perp$ shown in Table I were obtained from Eqs. (A9) and (A11).

The components B_{ij} of the F2 shf tensor were evaluated using a computerized least-squares fit in the same manner as for the Mn^{2+}-doped samples. The quality of the fit is indicated in Fig. 4 and the results are listed in Table II. No ^{57}Fe ENDOR could be detected.

In addition to the normal F1 ENDOR signals, including the resolved multiplet structure on the type-II transitions, a number of other ENDOR lines were observed whose angular dependence we interpret as indicating the presence of a nearby charge-compensating site along a ⟨111⟩-type direction. The details and interpretation of these ENDOR results will be presented in a forthcoming publication.

D. $KZnF_3:Ni^{2+}$ System

The Ni^{2+} ESR spectrum consists of a broad line on which are superimposed sharp double-quantum lines.[17,18] The width between peaks of the first-derivative curve was about 150 G for the broad line and about 5 G for the double-quantum lines at LHeT. The sign of the double-quantum first-derivative curves was found to be reversed[18,19] with respect to that of the broad line at LNT but not at LHeT. No Ni^{2+} ESR was observable at RT. Inability to saturate the ESR lines precluded ENDOR measurements, so the F1 shf constants were evaluated from the separations of the double-quantum lines. The results are included in Table I.

IV. DISCUSSION

As mentioned previously, Davies developed a model[7] in which the significant nondipolar part of the shf interaction between the F2 fluorines and the central magnetic ion D is ascribed to overlap between the F2 orbitals and the partially spin-polarized F1 orbitals. Davies neglects direct covalent effects on F2 as well as direct overlap between F2 wave functions and those of the magnetic ion.

The effect of this latter overlap integral can be shown by a numerical calculation to be negligibly small. The nondipolar part $\overleftrightarrow{a}$ of the F2 shf tensor $\overleftrightarrow{B}$ is most easily expressed in the starred coordinate system shown in Fig. 5. If $\overleftrightarrow{A}_d^*$ is the point dipolar interaction between F2 and D, then $\overleftrightarrow{a}^* \equiv \overleftrightarrow{B}^* - \overleftrightarrow{A}_d^*$. Since the isotropic part of the interaction makes the major contribution to the observed $\overleftrightarrow{a}^*$ in all the perovskite fluoride–magnetic-ion systems studied to date, and in order to simplify the discussion, we restrict our treatment to $\mathrm{tr}\,\overleftrightarrow{a}^*$. Our recalculation of Davies's formulas[7] yields the slightly modified result

$$\mathrm{tr}\,\overleftrightarrow{a}^* = \frac{3}{4S} A_{2s}[(f_\sigma + f_\pi)\langle s|Z^*\rangle^2 + 2f_s\langle s|S\rangle^2 - 2(2f_s f_\sigma)^{1/2}\langle s|S\rangle\langle s|Z^*\rangle] - \frac{15\kappa}{8S} A_{2p}[(f_\sigma + f_\pi)(\langle z^*|Z^*\rangle^2 + \langle x^*|X^*\rangle^2) + 2f_\pi\langle y|Y\rangle^2 + 2f_s\langle s|Z^*\rangle^2 + 2(2f_s f_\sigma)^{1/2}\langle s|Z^*\rangle\langle z^*|Z^*\rangle], \quad (3)$$

where the overlap integrals are written with the F1 and F2 orbitals represented by upper- and lower-case letters, respectively, the spin unpairing parameters f_i have their usual meaning (characterizing the corresponding unpaired antibonding hole),[2] and A_{2s} and A_{2p} are the hyperfine constants for a single unpaired $2s$ and $2p$ fluorine orbital, respectively.[2] Although we will use Eq. (3) for the purposes of calculation, a very good approximation is given by

$$\mathrm{tr}\,\overleftrightarrow{a}^* \simeq \frac{3}{4S} A_{2s}[(f_\sigma + f_\pi)\langle s|Z^*\rangle^2 - 2(2f_s f_\sigma)^{1/2}\langle s|S\rangle\langle s|Z^*\rangle]. \quad (4)$$

In evaluating the above overlap integrals, Davies and DH made use of the Sugano-Shulman[20] two-term analytical fits to Froese's[21] numerical Hartree-Fock $2s$ and $2p$ wave functions for F^-. Unfortunately, these fits do not yield accurate F1-F2 overlap integrals. In Table III, we compare the various overlap integrals[22] using the Froese-Sugano-Shulman (FSS) and Clementi[23] F^- wave functions for an undistorted F1-F2 distance in $KMgF_3$ (5.329 a.u.).

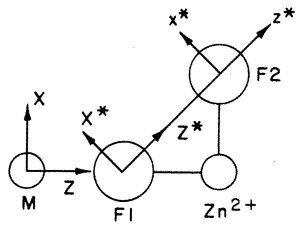

FIG. 5. Starred coordinate system used for computing the F1-F2 overlap integrals. X^*, Z^* refer to the F1 ion while x^*, z^* refer to F2.

TABLE III. Overlap integrals between nn and nnn fluorine ions in $KMgF_3$. Comparison of results using Froese-Sugano-Shulman (FSS) and Clementi wave functions.

Overlap integral	FSS	Clementi
$\langle s\|S\rangle$	0.0024	0.0065
$\langle s\|Z^*\rangle$	0.0282	0.0396
$\langle z^*\|Z^*\rangle$	−0.0703	−0.0684
$\langle x^*\|X^*\rangle$	0.0171	0.0224

The Clementi wave functions are the result of five-term Roothaan Hartree-Fock calculations, and they approximate the Froese results more closely than the FSS fits. Our calculations, using the F^- wave functions obtained by Sachs,[24] served to confirm the Clementi values. The use of Clementi rather than FSS wave functions strongly affects the value of $\mathrm{tr}\,\overleftrightarrow{a}^*$, as is shown in Table IV, where we compare the experimental and computed values. In general, the agreement between experiment and both sets of computations is poor, although the order of magnitude is roughly correct.

We digress momentarily to consider the details of the parameters used in the calculations of Table IV. The F1 and F2 ions are assumed to occupy their normal lattice positions and for the $KMgF_3$ case the f_i values of Refs. 7 and 8 were used. Using the ESR F1 results (Table I) as well as neutron-diffraction data [$(f_\sigma + 2f_\pi + f_s)(Mn^{2+}) = 3.3\%$ in MnF_2 (Ref. 25), $(f_\sigma + 2f_\pi + f_s)(Fe^{3+}) = 10.0\%$ in $LaFeO_3$ (Ref. 26)], we derive $f_s = 0.60\%$, $f_\sigma = 1.3\%$, and $f_\pi = 1.0\%$ for Mn^{2+} and $f_s = 0.78\%$, $f_\sigma = 5.3\%$, and $f_\pi = 1.5\%$ for Fe^{3+} in $KZnF_3$. To reflect the lesser covalency of the fluorides compared to the oxides we took $(f_s + f_\sigma + 2f_\pi)(Fe^{3+}) = 9\%$.

The new computations and the experimental results in Table IV make evident the following two trends. First, the value of $\mathrm{tr}\,\overleftrightarrow{a}^*$ computed on the overlap model is too large for the d^3 ions and too

TABLE IV. Experimental and overlap model values of $\mathrm{tr}\,\overleftrightarrow{a}^*$ for various impurity-host systems (units of MHz).

Host ion	$KMgF_3$[a]				$KZnF_3$[b]	
	V^{2+}	Cr^{3+}	Cr^{1+}	Mn^{2+}	Mn^{2+}	Fe^{3+}
$\mathrm{tr}\,\overleftrightarrow{a}^*$ (expt)	0.45	0.25	1.60	0.67	1.68	1.50
$\mathrm{tr}\,\overleftrightarrow{a}^*$ (this work, Clementi wave functions)	0.79	1.41	0.29	0.40	0.37	1.11
$\mathrm{tr}\,\overleftrightarrow{a}^*$[c] (FSS wave functions)	0.41	0.73[d]	0.15	0.22		

[a] Experimental values, Refs. 7 and 8.
[b] Experimental values, this work.
[c] Reference 8.
[d] There is apparently a typographical error for this quantity in Ref. 8.

small for the d^5 ions. Second, whenever a paramagnetic ion is replaced by a more highly charged isoelectronic ion the experimental value of tr $\overleftrightarrow{a}$* decreases, contrary to the effect expected from the concomitant increase in spin unpairing found on the F1 ions. On this latter point, our data for Mn^{2+} and Fe^{3+} in $KZnF_3$ extend the observation of DH. These workers invoked a local displacement of the F1 (and F2) ions toward the Cr^{3+} to obtain agreement for the isotropic as well as the anisotropic parts of $\overleftrightarrow{a}$* for that ion. However, this required a suspiciously large F1 displacement of 0.6 Å which, as DH themselves point out, should not be taken literally. The use of the more accurate Clementi wave functions compounds this difficulty since even larger F1 displacements are required to lower the F1-F2 overlap enough to restore agreement with experiment. Evidence can be marshaled to indicate that such large displacements do not actually occur for trivalent ions. In Fig. 6 we show the isotropic F1 hyperfine constant A_s for Fe^{3+} in several perovskite fluorides and also in K_2NaGaF_6 plotted as a function of the metal ion-F1 distance R in the host octahedral complex. Like Cr^{3+}, the Fe^{3+} ion has an excess positive charge in the perovskites and we can expect a contraction of the Fe^{3+}-F1 distance compared to that of the host lattice. In K_2NaGaF_6, however, any such contraction would be greatly reduced in magnitude because there is no charge mismatch. The

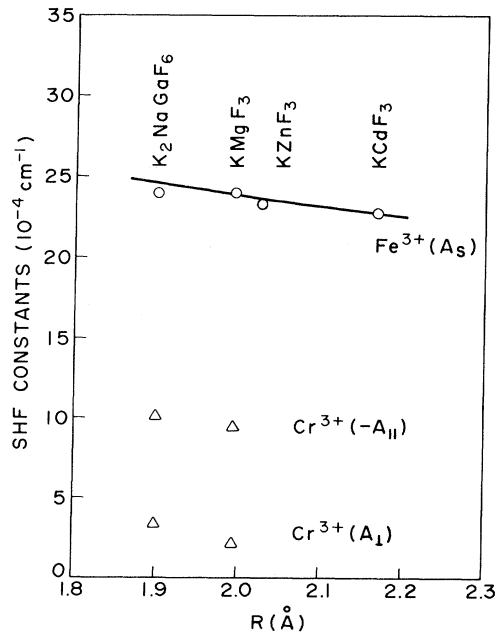

FIG. 6. F1 shf constants vs host-metal ion-F1 separation in several octahedral complexes. The $KZnF_3$ result is from this work (Table I), the other data are collected in Ref. 2.

fairly smooth variation of A_s with R argues strongly against any substantial F1 displacement in the perovskites. There are insufficient data available on Cr^{3+} to make a similar analysis, although ESR results for K_2NaGaF_6 suggest that no large displacement occurs around Cr^{3+} in $KMgF_3$ either (see Fig. 6).

Finally, we call attention to the large increase in tr $\overleftrightarrow{a}$* of Mn^{2+} on going from $KMgF_3$ to $KZnF_3$. Here the lattice constants are nearly the same (3.989 Å, $KMgF_3$; 4.040 Å, $KZnF_3$), so that there should be very little change in overlap or F1 displacement. It has been suggested[8] that the difference in tr $\overleftrightarrow{a}$* for Mn^{2+} in the two salts might be due to additional overlap paths involving the host (H) ions Mg^{2+} or Zn^{2+}. Such paths, however, would involve factors like $f_\sigma\langle F1|H\rangle^2\langle H|F2\rangle^2$ instead of $f_\sigma\langle F1|F2\rangle^2$ and should be negligible, as our detailed comparison of the relevant overlap integrals shows.[27] This result indicates the necessity of invoking covalency effects to explain the data. We conclude, based on the new overlap integrals and the above arguments, that although local displacement effects produce the proper trends in tr $\overleftrightarrow{a}$* vs the charge state of isoelectronic magnetic ions, the neglect of covalency and the use of ligand displacement as a free parameter in the overlap model is not supportable. Unfortunately, the local displacements which do occur near ions with a charge mismatch greatly complicate any attempt to evaluate the covalency effects for these complexes. Such evaluation would best be handled by comparing the same ion in two related hosts. To date, the only such case is Mn^{2+} in $KMgF_3$ and $KZnF_3$.

If one allows the possibility of covalent charge transfer between the F2 and Mn ions, the formula for tr $\overleftrightarrow{a}$* [Eq. (4)] is modified to read

$$\text{tr}\,\overleftrightarrow{a}^* \simeq (3/4S)\,A_{2S}\,[(\alpha_\pi\langle s|Z^*\rangle+\sqrt{2}\,\eta_{2s})^2+\eta_{5s}^2 + (\alpha_\sigma\langle s|Z^*\rangle+\sqrt{2}\,\alpha_s\langle s|S\rangle+\sqrt{2}\,\eta_{1s})^2]\,, \quad (5)$$

where $\eta_{is}=\gamma_{is}+\langle s|d_i\rangle$, γ_{is} is defined by the bonding orbital $|s\rangle_B=|s\rangle+\gamma_{is}|d_i\rangle$, and the α_i are the admixture coefficients for the F1 wave functions in the orthogonalized antibonding d_i hole orbitals. (Thus, $\alpha_i^2=f_i$ and the relevant subscripts are $1=z^2$, $2=zx$, $5=x^2-y^2$.)

There are too many new covalency parameters introduced to allow a determination of any one of them. However, to gain some idea of the magnitude of the required η_{is}, we make the simplifying assumption that all the η_{is} are zero except η_{1s}. Then we can compare Mn^{2+} in $KMgF_3$ and $KZnF_3$, neglecting displacement effects and assuming that the α_i and overlap integrals are constant. (Both of these assumptions are valid to a good approximation.) The value of η_{1s} required in Eq. (5) to give the observed values of tr $\overleftrightarrow{a}$* is then $\eta_{1s}=1.5\times10^{-3}$

for $KMgF_3$ and 5.0×10^{-3} for $KZnF_3$. These numbers are comparable in magnitude to the largest overlap term $\alpha_\sigma\langle s|Z^*\rangle = 4.4\times10^{-3}$, and the relative magnitudes of the η_{1s} are qualitatively what one expects because of smaller electronegativity difference (and thus greater covalency) between Zn and F as compared to Mg and F. The $\langle s|d_1\rangle$ overlap integral is less than 0.13×10^{-3}, so it is clear that $\eta_{1s}\simeq\gamma_{1s}$. Thus, invoking covalency to explain the tr $\overleftrightarrow{a}^*$ values for Mn^{2+} does lead to nontrivial values for the covalency parameter γ_{1s}. The theoretical justification of the order of magnitude found would require, however, an *ab initio* molecular orbital calculation which is outside the scope of the present investigation. It is clear, though, that such a calculation would have to include at least the nn divalent host metal ions in order to explain the rather large ratio tr $\overleftrightarrow{a}^*$ ($KZnF_3$: Mn)/tr $\overleftrightarrow{a}^*$ ($KMgF_3$: Mn).

In summary, it is seen from the experimental results to date that there are nontrivial isotropic spin densities at the nnn fluorine sites for $3d^3$ and $3d^5$ ions in perovskite fluorides. Furthermore, invoking only overlap between the F1 and F2 ions is inadequate to explain the data. The sign of the error is opposite for the $3d^3$ and the $3d^5$ ions and the results for Mn^{2+} in two different hosts imply that there are important covalency effects. Further progress in unraveling this problem would require a thoroughgoing theoretical treatment and/or additional measurements on the same ion in a pair of similar hosts (to cancel displacement effects). In particular, F2 ENDOR studies of V^{2+} in $KZnF_3$ seem to be indicated and additional work on Cr^+, Cr^{3+}, and Fe^{3+} could prove useful.

ACKNOWLEDGMENTS

The authors wish to thank V. J. Folen and R. A. Becker for the synthesis of the perovskite samples and H. A. Resing for furnishing his least-squares computer program.

APPENDIX

A. Spin-Hamiltonian Calculations for Cubically Symmetric System of D-$(F^-)_6$

The spin Hamiltonian appropriate to this type of complex may be written in the form

$$\mathcal{H} = g\,\mu_B\,\vec{H}\cdot\vec{S} + {}^DA\,\vec{I}\cdot\vec{S} + (\tfrac{1}{120}\,a)(O_4^0 + 5O_4^4) + \sum_i \vec{S}\cdot\overleftrightarrow{A}_i\cdot\vec{I}_i - {}^Dg_n\,\mu_N\,\vec{H}\cdot\vec{I} - \sum_i g_n\,\mu_N\,\vec{H}\cdot\vec{I}_i , \quad \text{(A1)}$$

where the various terms have the standard meanings[28,29] and the index i runs over the six fluorine nuclei that are nn to the $3d^n$ impurity ion denoted by D. For the iron-group transition-metal ions, S has the value $\frac{1}{2}$, 1, $\frac{3}{2}$, or $\frac{5}{2}$, depending on the ion, and the cubic field term a is nonzero only for $S=\frac{5}{2}$. The parameters g and ${}^DA$ are isotropic for the case considered.

The energy equations and resonant field values for the ESR transitions in this type of complex have been discussed by others.[12,28,30] We reiterate here the results appropriate to the present ESR and ENDOR study following the approach of KP[12] but using a more general zero-order Hamiltonian,

$$\mathcal{H} = g\,\mu_B\,HS_z + {}^DAS_zI_z + (\tfrac{1}{120}\,a)\,O_4^0 , \quad \text{(A2)}$$

as well as a perturbing Hamiltonian given by

$$\mathcal{H}_1 = A_\parallel S_z\sum_{i=1}^{2} I_{zi} + A_\perp S_z\sum_{i=3}^{6} I_{zi} + \frac{{}^DA}{2}(S^+I^- + S^-I^+) + \frac{a}{48}[(S^+)^4 + (S^-)^4] + C_xS_x + C_yS_y - {}^Dg_n\,\mu_N\,HI_z - g_n\,\mu_N\,H\sum I_{zi} . \quad \text{(A3)}$$

For $\vec{H}$ parallel to a cube edge of the $KZnF_3$ unit cell (the Z direction of Fig. 1) as assumed in Eqs. (A2) and (A3), the components of $\vec{C}$ are[12]

$$C_x = A_\parallel(I_{3x} + I_{5x}) + A_\perp(I_{1x} + I_{2x} + I_{4x} + I_{6x}) ,$$

$$C_y = A_\parallel(I_{4y} + I_{6y}) + A_\perp(I_{1y} + I_{2y} + I_{3y} + I_{5y}).$$

The components of the F1 shf tensor are given by

$$A_\parallel = A_s + 2(A_d + A_\sigma - A_\pi) ,$$

$$A_\perp = A_s - (A_d + A_\sigma - A_\pi) ,$$

in which A_s represents the isotropic part of the interaction due to spin unpairing in the fluorine s orbitals, $(A_\sigma - A_\pi)$ is the net contribution due to spin unpairing in the fluorine $2p_\sigma$ and $2p_\pi$ orbitals, and A_d is the contribution from the classical dipolar interaction between the electronic magnetic moment of the central D ion and the fluorine nuclear magnetic moment. For $\vec{H}\parallel[100]$ the nth-order energy perturbations E_n are

$$E_0(M, m) = g\,\mu_B\,HM + {}^DAMm + \tfrac{1}{2}\,aP(M) , \quad \text{(A4)}$$

$$E_1 = A_\parallel Mm_{\rm I} + A_\perp Mm_{\rm II} - {}^Dg_n\,\mu_N\,Hm - g_n\,\mu_N\,H(m_{\rm I} + m_{\rm II}) , \quad \text{(A5)}$$

$$E_2 = \tfrac{1}{4}({}^DA)^2\left(\frac{F(M)f(-m)}{\Delta(M-1,\ m+1)} + \frac{F(-M)f(m)}{\Delta(M+1,\ m-1)}\right) + \frac{5a^2}{4}\left(\frac{r(-M)}{\Delta(M-4,\ m)} + \frac{r(M)}{\Delta(M+4,\ m)}\right) - \mu_-(M)(A_\perp)^2 m_{\rm I} - \mu_-(M)\,A_\parallel A_\perp m_{\rm II} + \mu_+(M)\left[\tfrac{1}{2}(A_\parallel^2 + A_\perp^2)(U_{35} + U_{46}) + (A_\perp)^2 U_{12} + A_\parallel A_\perp(U_{34} + U_{45} + U_{56} + U_{63})\right] , \quad \text{(A6)}$$

$$E_3 = (A_\parallel m_{\rm I} + A_\perp m_{\rm II})\left[5a^2\left(\frac{r(M)}{\Delta^2(M+4, m)} - \frac{r(-M)}{\Delta^2(M-4, m)}\right) + \tfrac{1}{4}({}^DA)^2\left(\frac{F(M)f(-m)}{\Delta^2(M-1,\ m+1)} + \frac{F(-M)f(m)}{\Delta^2(M+1, m-1)}\right)\right], \quad \text{(A7)}$$

where $P(M) = \frac{1}{60} \langle M | 0_4^0 | M \rangle$,

$$m_{\rm I} = \sum_{i=1}^{2} I_{zi}\,,\quad m_{\rm II} = \sum_{i=3}^{6} I_{zi}\,,$$

$$F(\pm M) = S(S+1) - M(M \mp 1)\,,$$

$$f(\pm m) = I(I+1) - m(m \mp 1)\,,$$

$$\Delta(M', m') = E_0(M, m) - E_0(M', m')\,,$$

$$r(x) = \begin{cases} 1 & \text{for } x = +\frac{3}{2} \text{ or } +\frac{5}{2} \\ 0 & \text{otherwise}\,, \end{cases}$$

$$\mu_{\pm}(M) = \frac{1}{4}\left(\frac{F(M)}{\Delta(M-1, m)} \pm \frac{F(-M)}{\Delta(M+1, m)}\right)\,,$$

$$U_{ij} = I_i^+ I_j^- + I_i^- I_j^+\,.$$

Note that in Eqs. (A5)–(A7) the quantities $m_{\rm I}$, $m_{\rm II}$, and U_{ij} are still in operator form. The proper zero-order wave functions are listed in Ref. 12.

The ESR spectrum and the ENDOR frequencies for the nucleus of the D ion are obtained in a straightforward manner from the preceding energy equations using

$$h\nu_e = |E(M+1, m, m_{\rm I}, m_{\rm II}) - E(M, m, m_{\rm I}, m_{\rm II})|$$

and

$$h\nu_{\rm ENDOR} = |E(M, m+1, m_{\rm I}, m_{\rm II}) - E(M, m, m_{\rm I}, m_{\rm II})|,$$

respectively.

For the type-I fluorines, defined as those whose D-F 1 bond axis is along the applied field direction, the ENDOR spectrum consists of doublets whose components occur at frequencies given by

$$\nu_{\rm I} = \nu_{0\rm I} \pm \nu'\,, \tag{A8}$$

where

$$\nu_{0\rm I} = |MA_{\parallel} - \nu_L - (A_{\perp})^2\,\mu_-(M) + A_{\parallel}[\tfrac{1}{4}({}^DA)^2 F + 5a^2 R]|\,, \tag{A9}$$

with

$$F = \frac{F(M)f(-m) + F(-M)f(m)}{(g\mu_B H)^2}\,,$$

$$R = [r(M) - r(-M)]/(4g\mu_B H)^2\,, \tag{A10}$$

$$\nu' = (A_{\perp})^2\,\mu_+(M)\,.$$

For the type-II fluorines, defined as those whose D-F 1 bond axis is perpendicular to the applied field direction, the ENDOR spectrum consists of multiplets of at least eight lines split symmetrically about $\nu_{0\rm II}$, as was shown by KP.[12] When second- and third-order corrections are included, the expression for $\nu_{0\rm II}$ becomes

$$\nu_{0\rm II} = |MA_{\perp} - \nu_L - A_{\parallel}A_{\perp}\,\mu_-(M) + A_{\perp}[\tfrac{1}{4}({}^DA)^2 F + 5a^2 R]|\,. \tag{A11}$$

The multiplet structure lines occur at the frequencies given by[12]

$$\nu - \nu_{0\rm II} = \pm(\nu_1 + \nu_2)\,,\ \pm\tfrac{1}{3}(\nu_1 + \nu_2)\,,\ \pm(\nu_1 - \nu_2)\,,\ \pm\nu_1\,, \tag{A12}$$

where

$$\nu_1 = \tfrac{1}{2}(A_{\parallel}^2 + A_{\perp}^2)\,\mu_+(M)\,, \tag{A13a}$$

$$\nu_2 = 2A_{\parallel}A_{\perp}\,\mu_+(M)\,. \tag{A13b}$$

B. Resonance Equations for F 2 ENDOR

The ENDOR frequencies for the F 2 nuclei can be derived in first order from the nuclear Hamiltonian

$$\mathcal{H}_n = -g_n\,\mu_N\,\vec{\rm H}\cdot\vec{\rm I} + \sum_{ij} B_{ij}\,S_i\,I_j\,, \tag{A14}$$

where B_{ij} denotes the components of the F2 shf interaction tensor with the magnetic ion. A given component B_{ij} is the same for each F 2 nucleus, provided that B_{ij} is expressed in terms of the local coordinate system of each ion. Since the 24 F 2 nuclei are all related by symmetry, our computations make use of the fact that the B_{ij} for each nucleus may be expressed in terms of those for one reference nucleus, in particular, the ion labeled 1 in Fig. 1, whose local coordinates are chosen identical with the unit-cell coordinate system (X, Y, Z). In our experiment, where the applied magnetic field was confined to the X-Z plane, there were only eight distinguishable types of F 2 ions—those labeled 1 through 8 in Fig. 1. (Nuclei labeled 3a and 3b are equivalent for such field directions.) Under the condition that $\vec{\rm S}$ is quantized along the applied field $\vec{\rm H}$ while $\vec{\rm I}$ is quantized along the effective field $\vec{\rm H}_{\rm eff}$, from Eq. (A14) it can be shown that the ENDOR frequencies are given by

$$\nu^2 = \textstyle\sum_j (\nu_L\,\alpha_j - M\sum_i B_{ij}\,\alpha_i)^2\,, \tag{A15}$$

where the α_i are the direction cosines of $\vec{\rm H}$ with respect to (X, Y, Z), ν_L is the fluorine Larmor frequency, and B_{ij} is expressed in frequency units. From Eq. (A15) the ENDOR frequency for ion 1 is

$$\nu_1^2 = (\nu_L \sin\theta - B_{xx}M\sin\theta - B_{zx}M\cos\theta)^2 + (\nu_L\cos\theta - B_{xz}M\sin\theta - B_{zz}M\cos\theta)^2\,, \tag{A16}$$

while the ENDOR frequencies for ions 2, 3, and 4 are given, respectively, by

$$\nu_2^2 = (\nu_L \sin\theta - B_{xx}M\sin\theta + B_{zx}M\cos\theta)^2 + (\nu_L\cos\theta + B_{xz}M\sin\theta - B_{zz}M\cos\theta)^2\,, \tag{A17}$$

$$\nu_3^2 = (\nu_L \sin\theta - B_{yy}M\sin\theta)^2 + (B_{zx}M\cos\theta)^2 + (\nu_L\cos\theta - B_{zz}M\cos\theta)^2\,, \tag{A18}$$

$$\nu_4^2 = (\nu_L \sin\theta - B_{zz}M\sin\theta - B_{xz}M\cos\theta)^2 + (\nu_L\cos\theta - B_{zx}M\sin\theta - B_{xx}M\cos\theta)^2\,, \tag{A19}$$

where θ is the angle between $\vec{H}$ and the Z direction. Since in our experiments only the above transitions were sufficiently resolved from the clutter of lines near ν_L to be identified with certainty, it is not useful to write down the ENDOR frequency expressions for the other F2 ions.

---

*NAS-NRC Postdoctoral Research Associate.

[1]J. Owen and K. W. H. Stevens, Nature 171, 836 (1953).

[2]J. Owen and J. H. M. Thornley [Rept. Progr. Phys. 29, 675 (1966)] provide an excellent critical review.

[3]H. A. Kiska and M. T. Rogers, in *Radical Ions*, edited by E. T. Kaiser and L. Kevan (Interscience, New York, 1968), pp. 579–746. This review contains 1057 references.

[4]D. E. Ellis, A. J. Freeman, and P. Ros, Phys. Rev. 176, 688 (1968).

[5]D. E. Rimmer, J. Phys. C 2, 329 (1969).

[6]P. W. Anderson, in *Solid State Physics*, edited by F. Seitz and D. Turnbull (Academic, New York, 1963), Vol. 14, p. 99.

[7]J. J. Davies, J. Phys. C 1, 849 (1968).

[8]J. J. Davies and K. Horai, J. Phys. C 4, 671 (1971); 4, 682 (1971).

[9]R. K. Jeck, J. J. Krebs, and V. J. Folen, J. Appl. Phys. 41, 1116 (1970).

[10]A. R. Cook, L. M. Matarrese, and J. S. Wells, Rev. Sci. Instr. 35, 114 (1964).

[11]J. P. Gordon, Rev. Sci. Instr. 32, 658 (1961).

[12]L. C. Kravitz and W. W. Piper, Phys. Rev. 146, 322 (1966).

[13]D. J. I. Fry, P. M. Llewellyn, and M. H. L. Pryce, Proc. Roy. Soc. (London) A266, 84 (1962).

[14]J. Ferguson, D. L. Wood, and K. Knox, J. Chem. Phys. 39, 881 (1963).

[15]W. T. Doyle and T. F. Dutton, Phys. Rev. 180, 424 (1969).

[16]E. R. Davies and T. R. Reddy, Phys. Letters 31A, 398 (1970).

[17]T. P. P. Hall, W. Hayes, R. W. H. Stevenson, and J. Wilkins, J. Chem. Phys. 38, 1977 (1963).

[18]J. W. Orton, P. Auzins, and J. E. Wertz, Phys. Rev. Letters 4, 128 (1960).

[19]Z. Sroubek, Czech. J. Phys. B 11, 634 (1961).

[20]S. Sugano and R. G. Shulman, Phys. Rev. 130, 517 (1963).

[21]C. Froese, Proc. Cambridge Phil. Soc. 53, 206 (1957).

[22]Calculated using a program by A. C. Switendick and F. J. Corbato; Program 138, Quantum Chemistry Program Exchange, Indiana University, modified by J. Jesaitis (unpublished).

[23]E. Clementi and A. D. McLean, Phys. Rev. 133, A419 (1964).

[24]L. M. Sachs, Phys. Rev. 124, 1283 (1961).

[25]R. Nathans, G. Will, and D. E. Cox, in *Proceedings of the International Conference on Magnetism, Nottingham* (The Institute of Physics and the Physical Society, London, 1965), p. 327.

[26]B. C. Tofield and B. E. F. Fender, J. Phys. Chem. Solids 31, 2741 (1970).

[27]Wave functions for Zn^{2+}, Mg^{2+}, and K^{+} obtained from E. Clementi, IBM J. Res. Develop. Suppl. 9, 2 (1965).

[28]W. Low, in *Solid State Physics*, edited by F. Seitz and D. Turnbull (Academic, New York, 1960), Suppl. 2.

[29]M. T. Hutchings, in *Solid State Physics*, edited by F. Seitz and D. Turnbull (Academic, New York, 1960), Vol. 16, pp. 227–272.

[30]J. Schneider and S. R. Sircar, Z. Naturforsch. 17a, 570 (1962).